Am J Nucl Med Mol Imaging 2024;14(2):134-143
www.ajnmmi.us /ISSN:2160-8407/ajnmmi0154464

Original Article

Subregion-specific ^{18}F-FDG PET-CT radiomics for the pre-treatment prediction of EGFR mutation status in solid lung adenocarcinoma

Yun Wang[1*], Guang Yang[2*], Xinyi Gao[3], Linfa Li[1], Hongzhou Zhu[3], Heqing Yi[1]

[1]Department of Nuclear Medicine, Zhejiang Cancer Hospital, Hangzhou 310022, Zhejiang, China; [2]Department of Physics, Shanghai Key Laboratory of Magnetic Resonance, East China Normal University, Shanghai 200062, China; [3]Department of Radiology, Zhejiang Cancer Hospital, Hangzhou 310022, Zhejiang, China. [*]Equal contributors.

Received November 17, 2023; Accepted March 7, 2024; Epub April 25, 2024; Published April 30, 2024

Abstract: This study aimed to assess the efficacy of fluor-18 fluorodeoxyglucose (^{18}F-FDG) PET/CT using sub-regional-based radiomics in predicting epidermal growth factor receptor (EGFR) mutation status in pretreatment patients with solid lung adenocarcinoma. A retrospective analysis included 269 patients (134 EGFR+ and 135 EGFR-) who underwent pretreatment ^{18}F-FDG PET/CT scans and EGFR mutation testing. The most metabolically active intratumoral sub-region was identified, and radiomics features from whole tumors or sub-regional regions were used to build classification models. The dataset was split into a 7:3 ratio for training and independent testing. Feature subsets were determined by Pearson correlation and the Kruskal Wallis test and radiomics classifiers were built with support vector machines or logistic regressions. Evaluation metrics, including accuracy, area under the curve (AUC), sensitivity, specificity, positive predictive value (PPV), and negative predictive value (NPV) were employed for different classifiers. Results indicated that the sub-region-based classifier outperformed the whole-tumor classifier in terms of accuracy (73.8% vs. 66.2%), AUC (0.768 vs. 0.632), specificity (65.0% vs. 50.0%), PPV (70.2% vs. 62.2%), and NPV (78.8% vs. 74.0%). The clinical classifier exhibited an accuracy of 75.0%, AUC of 0.768, sensitivity of 72.5%, specificity of 77.5%, PPV of 76.3%, and NPV of 73.8%. The combined classifier, incorporating sub-region analysis and clinical parameters, demonstrated further improvement with an accuracy of 77.5%, AUC of 0.807, sensitivity of 77.5%, specificity of 77.5%, and NPV of 77.5%. The study suggests that sub-region-based ^{18}F-FDG PET/CT radiomics enhances EGFR mutation prediction in solid lung adenocarcinoma, providing a practical and cost-efficient alternative to invasive EGFR testing.

Keywords: Radiomics, epidermal growth factor receptor, solid lung adenocarcinoma, ^{18}F-FDG PET/CT, prediction

Introduction

Lung cancer represents a ubiquitous and highly consequential global health challenge, characterized by the highest rates of both mortality and morbidity on a worldwide scale. Non-small cell lung cancer (NSCLC) constitutes approximately 85% of all diagnosed lung cancer cases [1, 2]. NSCLC harboring epidermal growth factor receptor (EGFR) mutations exhibits heightened responsiveness to EGFR tyrosine kinase inhibitors (TKIs), constituting a targeted therapeutic approach. Implementation of EGFR-targeted therapy holds the promise of enhancing both median overall survival (OS) and progression-free survival (PFS) for patients within this particular subset [3]. Initial EGFR gene testing before treatment has been recommended by several clinical guidelines [4]. The prevailing clinical protocol for EGFR genotyping relies on biopsy procedures, a methodology fraught with potential technical constraints such as insufficient tissue availability, complications associated with invasive biopsy, and the inherent risk of procedural complications [5].

Genotypic heterogeneity significantly influences the diversity observed in the tumor microenvironment, encompassing aspects such as tumor metabolism, which can manifest in imaging modalities. ^{18}F-FDG positron emission tomography (PET) relies on varying rates of ^{18}F-FDG uptake, and in the context of lung cancer cells with EGFR mutations, the uptake of ^{18}F-FDG may be modulated by the signaling activity of the EGFR pathway [6]. The incorporation of ^{18}F-FDG PET/computed tomography (CT), a hybrid imaging modality that integrates ^{18}F-FDG PET for the quantitative assessment of glucose metabolism with CT for X-ray absorption detection, is advocated for the routine staging of patients diagnosed with lung adenocarcinoma as an integral component of the initial clinical evaluation. While prior investigations employing ^{18}F-FDG PET/CT to predict gene mutations in lung cancer have predominantly centered on visual analysis or conventional semi-quantitative parameters, such as standardized uptake values (SUVs) [7, 8], without considering CT information and various textures reflecting heterogeneity [8]. With the application of medical artificial intelligence, it has become feasible to find fast, convenient, and noninvasive surrogates for EGFR genotyping. Quantitative imaging analysis employing radiomics methodology has the capacity to extract a robust set of objective and high-throughput imaging features from provided images, facilitating automated gene prediction. Consequently, radiomics holds promise for its application in genotyping within the context of ^{18}F-FDG PET/CT.

Previous radiomics analysis usually set the whole tumor volume as the region of interest (ROI). However, many

https://doi.org/10.62347/DDRR4923

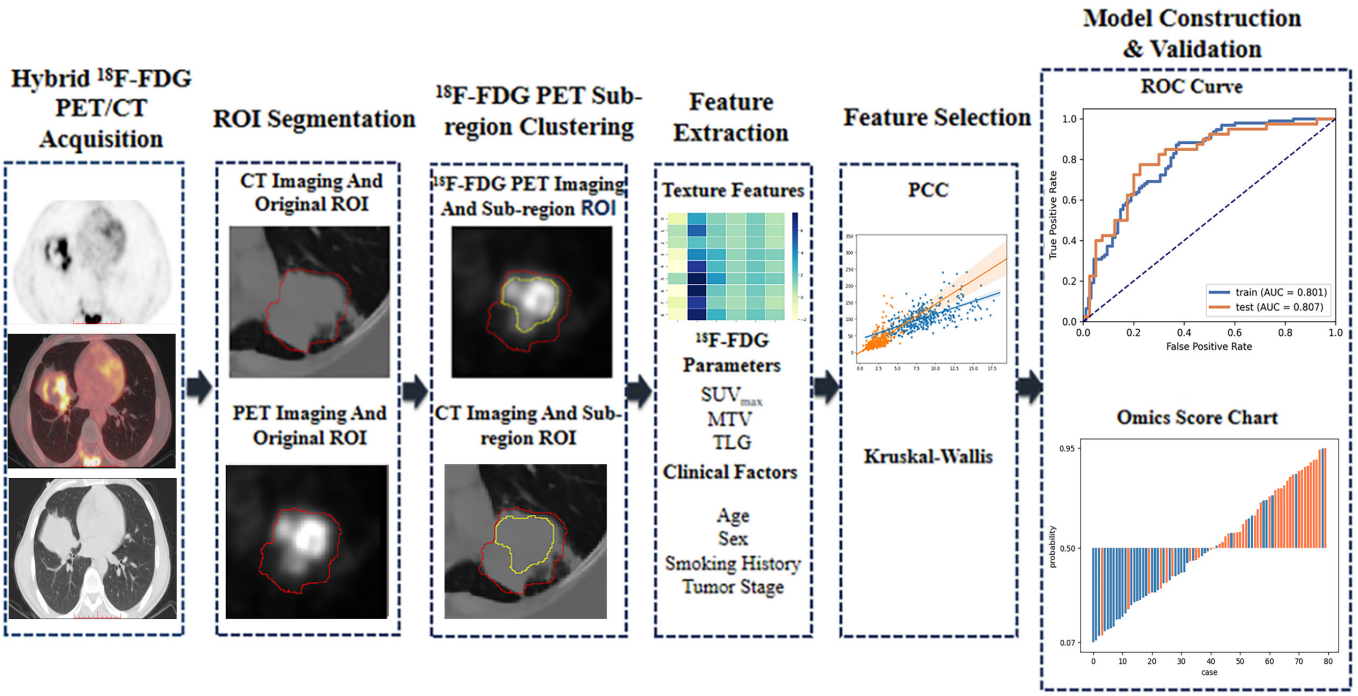

Figure 1. The workflow employed in this study.

studies have found that information from different sub-regions of the tumor contributes differently to classification. Whole tumor analysis assumes that the tumor is homogeneous or well mixed throughout the whole volume. In addition, regional differences are apparent within the whole tumor on medical images, such as ^{18}F-FDG PET. In recent years, efforts have been made in developing imaging analysis based on sub-regions instead of whole tumors [9, 10]. Regional disparities within the tumor may manifest distinct metabolic patterns on ^{18}F-FDG PET, thereby suggesting that information derived from specific sub-regions could serve as valuable indicators for the assessment of tumor heterogeneity and genotype.

A study conducted by Stanford University demonstrated that the metabolically most active sub-region, as identified through FDG PET, can function as a reliable predictor of overall survival (OS) and progression outside the treatment field in patients with previously treated lung cancer [11]. Therefore, radiomics features can be used along with other clinical data to improve diagnostic accuracy.

We postulated that the EGFR genetic profile of solid lung adenocarcinomas could be discerned in their phenotypic and metabolic traits, and that these characteristics could be more effectively elucidated through radiomics analysis employing sub-regions in ^{18}F-FDG PET/CT. Our goal was to formulate an innovative integrated radiomics classifier for predicting EGFR mutation status in patients with solid lung adenocarcinoma before treatment. This classifier incorporates both metabolic and anatomical information extracted from the most metabolically dynamic sub-region within the tumor on ^{18}F-FDG PET/CT, alongside clinical information.

Materials and methods

This single-center analysis was approved by institutional ethic committee (IRB-2020-207) and individual written informed consent for this retrospective analysis was waived.

Patient selection

The workflow of this study is displayed in **Figure 1**. We retrospectively reviewed patients with histologically proven lung adenocarcinoma who underwent pretherapy ^{18}F-FDG PET/CT scan between December 2016 and December 2020 in Zhejiang cancer hospital. The inclusion criteria were (1) pathologically confirmed adenocarcinoma according to the latest guidelines [12]; (2) presence of solid lung lesion on pretreatment ^{18}F-FDG PET/CT; (3) EGFR mutation tested by real-time fluorescence polymerase chain reaction (PCR); (4) < 1 months between ^{18}F-FDG PET/CT scan and gene alteration detection; (5) no anti-tumor treatment received before PET/CT examination; and (6) no history of other malignant tumors. The exclusion criteria were (1) patients with rare EGFR mutations in exons other than between exons 18-21; (2) pure ground-glass nodule without ^{18}F-FDG uptake and subsolid pulmonary nodule; (3) patients with chest active infections such as pneumonia that could confound ^{18}F-FDG analysis.

EGFR mutation testing

In patients with stages 1-3 (n=102, 37.9%), EGFR mutation analysis was performed on histological specimens obtained through surgical resection using real-time fluo-

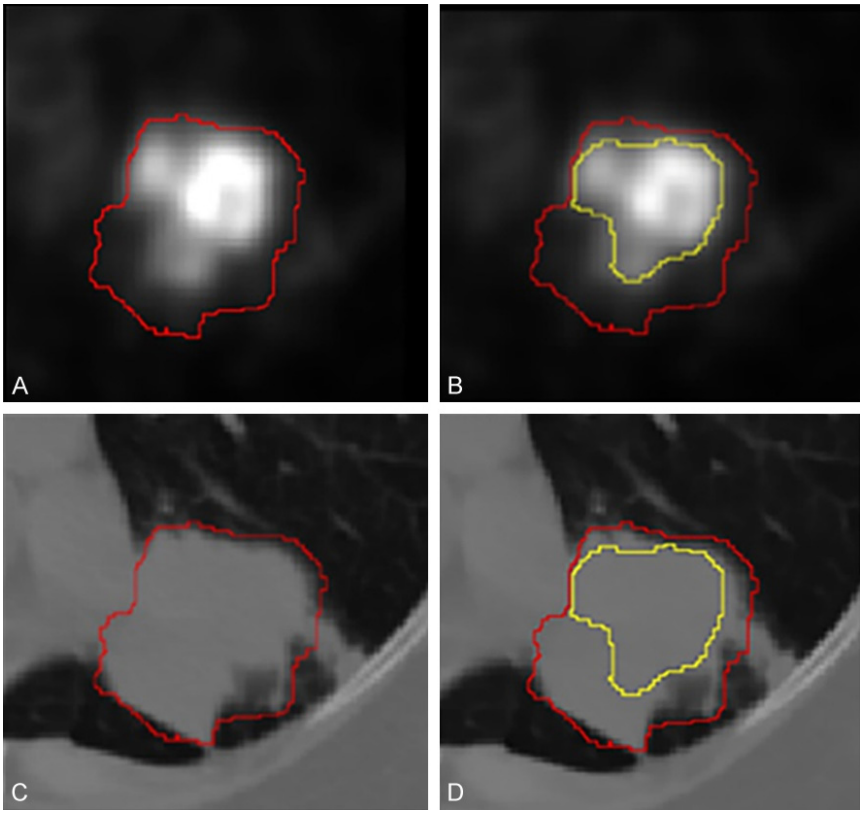

Figure 2. An illustrative example of tumor segmentation for a patient. In the PET images, the whole-tumor ROI is delineated in red, and the sub-region ROI is highlighted in yellow (A and B). Likewise, in the CT images, the whole-tumor ROI is marked in red, and the sub-region ROI is indicated in yellow (C and D).

rescence PCR with the EGFR Mutations Detection Kit (Human EGFR gene mutation detection kit, AmoyDx, Xiamen, Fujian, China), and the outcome was interpreted following the manufacturer's instructions. For patients in stage 4 (n=167, 62.1%), the specimens submitted for EGFR mutational analysis were predominantly acquired through CT-guided core-needle biopsy (n=125, 74.9%); The remaining specimens were acquired through ultrasound-guided percutaneous biopsy (n=42, 25.1%). If any mutation in EGFR exon 18-21 was detected, the subject was considered to be an EGFR mutant. Otherwise, the tumor was considered as EGFR wild type.

Image acquisition

The imaging acquisition protocol was established following the Image Biomarker Standardization Initiative (IBSI) reporting guidelines [13]. ^{18}F-FDG PET/CT imaging was conducted utilizing the Discovery 710 PET/CT system (GE Medical Systems, Milwaukee, Wisconsin, USA). Patients were instructed to fast for at least 6 h before the PET scan. Blood glucose level was measured to ensure that it was < 200 mg/dL. ^{18}F-FDG was administered intravenously at a dosage of 3.7 MBq/kg. ^{18}F-FDG PET/CT scan was performed within 1 month before treatment. In short, ^{18}F-FDG PET/CT images were acquired 60 ± 5 min after ^{18}F-FDG injection in accordance with the European Association of Nuclear Medicine guidelines, version 2.0 [14]. Attenuation correction CT was conducted with the following parameters: 120 kV, 150 mA, slice thickness: 3 mm. Subsequently, the PET scan was promptly acquired from the head to the upper leg, with a duration of 3 minutes per bed position. Typically, 6-8 bed positions were surveyed, adjusting as per the patient's height. The PET images were reconstructed employing the ordered set expectation maximization algorithm. The attenuation correction of PET images was carried out with CT data, and the corrected PET images were fused with CT images. The PET parameters computed in 3D mode using vendor-provided software included: metabolic tumor volume (MTV), maximum SUV (SUV_{max}), total lesion glycolysis (TLG), and mean SUV (SUV_{mean}). The MTV for each solid lung adenocarcinoma lesion was assessed utilizing the adaptive threshold method. This involved selecting a volume of interest (VOI) on the axial image, and the size of the VOI was verified using corresponding coronal and sagittal images to encompass the entire lesion. The TLG was computed by multiplying the SUV_{mean} by the MTV.

ROI segmentation and sub-region clustering

All lesions on CT were initially and manually contoured slice by slice by 2 radiologists (reader 1: YW with 12 years of experience; reader 2: XYG with 10 years of experience) using ITKSNAP (http://www.itksnap.org) and then scrutinized by a radiology specialist (HZZ, with 27 years of experience). Based on the method of Wu et al. [15], we further tested intra- and inter-observer reproducibility. Therefore, an intra-class correlation coefficient > 0.75 was considered to indicate satisfactory reproducibility. In this study, the segmentation of sub-regional Regions of Interest (ROIs) is performed using Otsu's thresholding method, which divides an image into two classes, foreground and background, based on the grayscale intensity values of its pixels. This segmentation technique is implemented through the utilization of the open-source Python package, scikit-image, to automatically delineate sub-regional ROIs. The process involves leveraging Otsu's thresholding method to efficiently separate image components, and this implementation is facilitated using the scikit-image library for enhanced precision and automation (https://scikit-image.org/docs/dev/api/skimage.filters.html#skimage.filters.threshold_otsu). **Figure 2** illustrates an example of whole-tumor ROI and sub-region ROI.

Feature extraction, selection and model construction

We applied normalization to the feature matrix. Radiomic features were extracted from each whole-tumor ROI and

sub-region ROI with Pyradiomics (http://pyradiomics.readthedocs.io/en/latest/index.html). Shape features, together with grayscale and texture features from the original image, wavelet transform, and LoG hyper-parameters (lambda =1.0, 3.0, 5.0) filtered images were extracted.

Texture features encompassed various types, including Gray Level Co-occurrence Matrix (GLCM), Gray Level Size Zone Matrix (GLSZM), Gray Level Run Length Matrix (GLRLM), Neighboring Gray Tone Difference Matrix (NGTDM), and Gray Level Dependence Matrix (GLDM). The primary objectives encompass addressing imbalances in the training dataset via the Synthetic Minority Oversampling Technique (SMOTE) and each feature vector underwent a normalization process by subtracting its mean value and dividing by the module of the vector. Given the discrepancy between the relatively small sample size and the high-dimensional feature size, dimension reduction and feature selection were executed. For each feature exhibiting a Pearson correlation coefficient (PCC) value of > 0.99, one of them was randomly omitted, resulting in a reduction of the feature space dimension and mitigating feature redundancy.

Before model construction, measures were taken to eliminate highly correlated features, reduce dimensionality through feature selection using Kruskal Wallis, and utilize logistic regression as the classifier. The F-value was calculated to evaluate the relationship between features and the label. Features were classified depending on the corresponding F-value and top N features were determined through cross-validation with 5-fold on the training dataset based on the model's performance on the validation dataset. Classifier 1 was built based on features extracted from the whole-tumor ROIs. Classifier 2 was built based on features extracted from the sub-regional ROIs. Classifier 3 was a clinical model (gender, age, TNM stage, smoking history, MTV, TLG, and SUV_{max}). Classifier 2 and 3 prediction probabilities were combined for building model 4. We used a support vector machine (SVM) with a linear kernel - an effective and robust classifier that searches the hyperplane to separate the cases with different labels - to build classifier 1 and 2. We used the linear kernel for its simplicity and interpretability. For classifier 3 and 4, we adopted logistic regression, which is a linear classifier that combines all features. To determine the number of retained features in each model, a 5-fold cross-validation was performed on training dataset, and the final features number was set according to cross-validation results.

Prognostic performance evaluation

The area under receiver operation characteristic (ROC) curve (AUC) value were computed to evaluate and compare the prediction performance. Meanwhile, other quantitative evaluation indices involving accuracy, sensitivity, specificity, positive predictive value (PPV), and negative predictive value (NPV) were also computed to evaluate the prediction performance. In addition, we estimated the 95% confidence interval by bootstrapping with 1000 samples. All the above processes were implemented with FeAture Explorer (FAE, V 0.3.6) on Python (3.7.6) [16].

Results

Patient characteristics

Based on the provided criteria, a total of 269 patients diagnosed with lung adenocarcinoma were enrolled in this study. The cohort comprised 155 males and 114 females, with an average age of 63.0 ± 11.0 years (range from 29 to 89). Among the participants, 134 cases exhibited EGFR mutation, constituting 49.8% of the total, while 135 cases were classified as EGFR wild type, representing the remaining 50.2%. The proportion of female patients with EGFR mutations is higher than that of males (56.0% vs. 44.0%). Additionally, EGFR wild-type patients exhibit a higher prevalence of smoking history compared to EGFR mutant patients (62.2% vs. 33.6%). EGFR wild-type patients demonstrate significantly elevated SUV_{max}, MTV, and TLG compared to EGFR mutant patients, with all differences reaching statistical significance (all $P < 0.05$). There were no statistically significant differences in age and TNM staging between EGFR mutant and wild-type groups (both $P > 0.05$), as shown in **Table 1**. Representative ^{18}F-FDG PET/CT images of patients with EGFR mutations and wild-type are illustrated in **Figure 3**. The clinical characteristics of the patients are summarized in **Table 1**.

Feature selection, model establishment and evaluation

269 patients were randomly split into the training set (EGFR mutant: 94; EGFR wild type: 95; total: 189) and the testing set (EGFR mutant: 40; EGFR wild type: 40; total: 80).

Classifier 1: SVM training and testing based on whole-tumor ROI: In the SVM training and testing phase, exclusive attention was directed towards features originating from whole-tumor ROIs. Through meticulous scrutiny, the classifier discerned the top 12 features from a comprehensive pool of 1130, culminating in the development of an SVM classifier exhibiting a diagnostic accuracy of 66.2% in the test cohort. The AUC was computed as 0.733 in the training cohort. The comprehensive performance metrics of the whole-tumor classifier included an accuracy of 66.2%, AUC of 0.632 (95% CI: 0.507-0.763), sensitivity at 82.5%, specificity at 50.0%, PPV at 62.2%, and NPV at 74.0%. The acquisition of diagnostic proficiency for EGFR mutation status through the SVM classifier based on Whole-Tumor ROIs is underscored by these results, elucidating its capability to effectively categorize instances within the evaluated datasets. The ROC curve for classifier 1 is visually depicted in **Figure 4A**.

Classifier 2: SVM training and testing based on sub-region ROI: In this phase of the study, SVM classifier training and testing were exclusively conducted utilizing features

Table 1. Demographics and clinicopathologic characteristics of eligible lung adenocarcinoma patients with EGFR mutation status included in this study

	Total	Mutant EGFR	Wild type EGFR	*p* value
Number	269	134	135	
Age, median years (range)	64 (29-89)	63 (29-82)	65 (30-89)	0.082
Smoking history (yes)	129 (48.0%)	45 (33.6%)	84 (62.2%)	< 0.001
Sex				< 0.001
Male	155 (57.6%)	59 (44.0%)	96 (71.1%)	
Female	114 (42.4%)	75 (56.0%)	39 (28.9%)	
Stage				0.980
I-II	38 (14.1%)	19 (14.2%)	19 (14.1%)	
III-IV	231 (85.9%)	115 (85.8%)	116 (85.9%)	
Diameter, cm				
SUV_{max}, mean ± SD		10.6 ± 4.9	14.0 ± 6.0	< 0.001
MTV, mean ± SD		10.4 ± 14.0	19.1 ± 23.3	< 0.001
TLG, mean ± SD		74.2 ± 109.5	164.7 ± 204.1	< 0.001

EGFR, epidermal growth factor receptor; SUV_{max}, maximum standardized uptake value; MTV, metabolic tumor volume; TLG, total lesion glycolysis. $P < 0.05$ was considered to indicate a statistically significant difference.

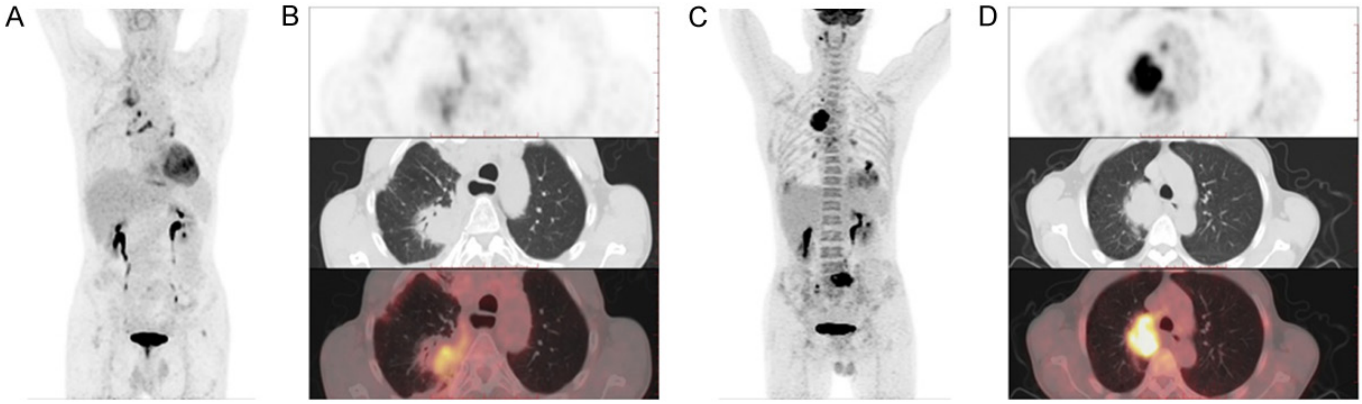

Figure 3. The image illustrates representative ^{18}F-FDG PET/CT images of patients with EGFR mutant and wild-type status. Patient 1, male, 64 years old, tested positive for EGFR mutation. The fused PET/CT images reveal an approximately 3.2 cm diameter lesion in the right upper lobe of the lung, exhibiting increased radioactive uptake with SUV_{max}=6.8, MTV=6.8, and TLG=27.2 (A and B). Patient 2, male, 62 years old, tested negative for EGFR mutation. The fused PET/CT images display an approximately 4.9 cm diameter lesion in the right upper lobe of the lung, showing elevated radioactive uptake with SUV_{max}=18.3, MTV=23.7, and TLG=228.3 (C and D).

extracted from sub-regions. The classifier strategically identified and employed the top 17 features from a comprehensive set of 1130 features. Within the training cohort, the SVM model achieved an AUC of 0.774 and accuracy of 0.682 for the diagnosis of EGFR status. Subsequently, the SVM classifier demonstrated notable performance metrics in the independent test cohort, registering an accuracy of 73.8%, an AUC of 0.768 (95% CI: 0.657-0.871), sensitivity at 82.5%, specificity at 65.0%, PPV at 70.2%, and NPV at 78.8%. These findings underscore the efficacy of the sub-region classifier in discerning and accurately categorizing instances within the examined datasets. **Figure 4B** illustrates the ROC curve of classifier 2.

Classifier 3: clinical model: Following the preprocessing procedures and feature selection steps in the development of the classification model, feature parameters for the clinical model were determined. The clinical model was trained using clinical variables (gender, age, smoking history, and TNM stage) along with PET parameters. ROC curve analysis was employed to assess the predictive efficacy of the clinical model in diagnosing EGFR mutations. This model exhibited an AUC of 0.753, accuracy of 66.7% in the training cohort. In the independent test cohort, the clinical classifier demonstrated metrics with values of 75.0% accuracy, AUC of 0.768 (95% CI: 0.658-0.868), sensitivity at 72.5%, specificity at 77.5%, PPV at 76.3%, and NPV at 73.8%. The ROC curve of classifier 3 is visually depicted in **Figure 4C**, providing a graphical representation of the classifier's discriminative performance.

Classifier 4: combined model: In this methodology, the prediction probabilities generated by classifier 2 and 3 were utilized to train a combined model. Following the preprocessing and feature selection steps in the develop-

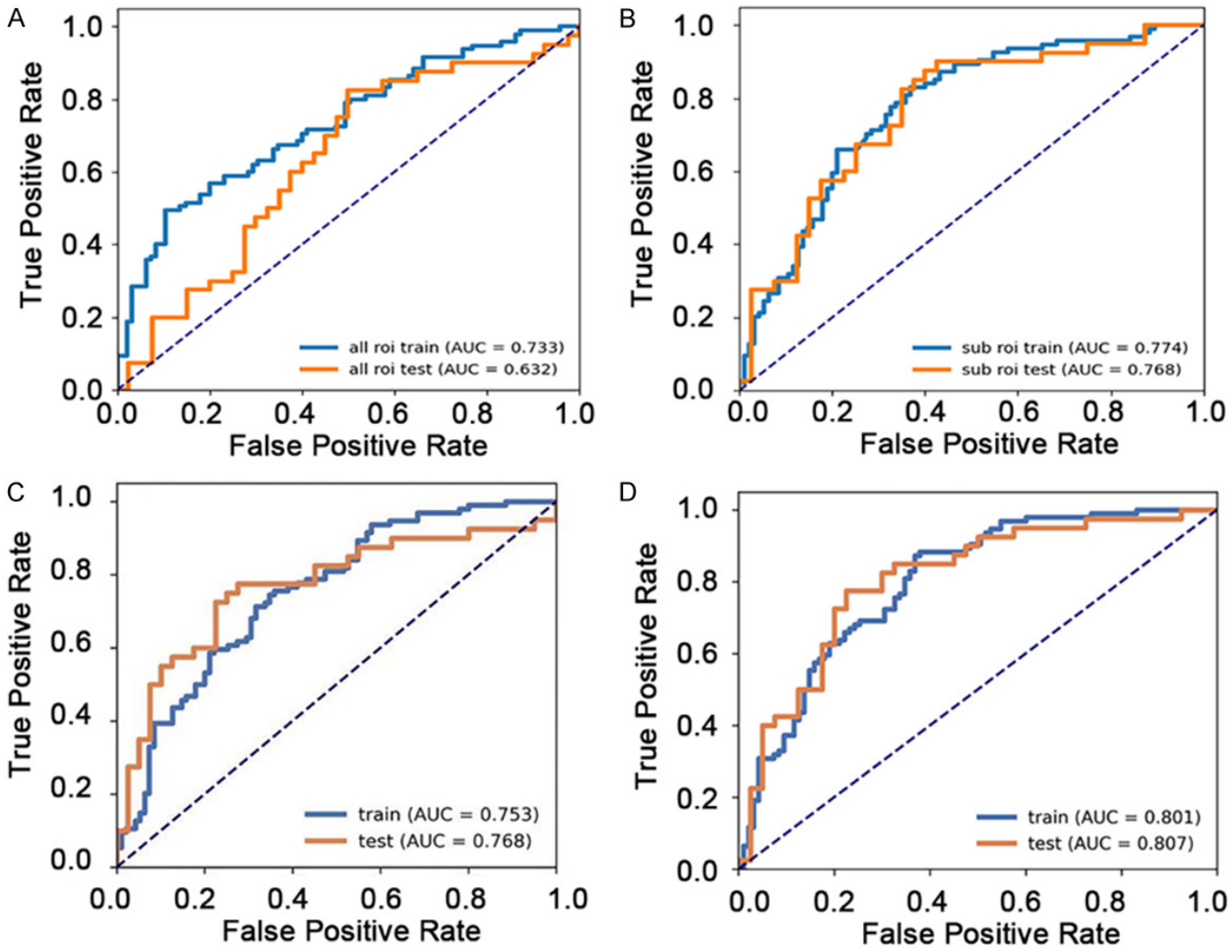

Figure 4. ROC curves for four distinct models predicting EGFR mutations. ROC curve for classifier 1 using whole-tumor ROI (A). ROC curve for classifier 2 using sub-regional ROI (B). ROC curve for classifier 3 based on the clinical model (C). ROC curve for classifier 4 representing the combined model (D).

Table 2. Comparison of the model performance in terms of different evaluation

Models	Accuracy	AUC	95% CI	NPV	PPV	Sensitivity	Specificity
Classifier 1	0.662	0.632	0.507-0.763	0.740	0.622	0.825	0.500
Classifier 2	0.738	0.768	0.657-0.871	0.788	0.702	0.825	0.650
Classifier 3	0.750	0.768	0.658-0.868	0.738	0.763	0.725	0.775
Classifier 4	0.775	0.807	0.699-0.896	0.775	0.775	0.775	0.775

AUC, area under curve; CI, confidence interval; PPV, positive predictive value; NPV, negative predictive value; Classifier 1, whole-tumor ROI based model; Classifier 2, sub-regional ROI based model; Classifier 3, clinical model; Classifier 4, combined model.

ment of the combined model, the classifier discerned the top two features from a pool of 1130. The performance of the model in predicting EGFR mutation status was assessed using ROC curve analysis, revealing that the model based on these two features achieved the highest AUC in the test cohort. In the training cohort, the combined model demonstrated an AUC of 0.801, accompanied by an accuracy of 0.730. For the combined classifier, which integrates sub-region analysis parameters and clinical parameters, the performance metrics in the independent test cohort were as follows: an accuracy of 77.5%, an AUC of 0.807 (95% CI: 0.699-0.896), and both sensitivity and specificity at 77.5%. Additionally, the positive predictive value (PPV) and negative predictive value (NPV) were both registered at 77.5%. **Figure 4D** visually depicts the ROC curve of classifier 4, while **Table 2** provides a detailed representation of the performance of different classifiers.

Discussion

In the standard care protocol for pretreatment of NSCLC patients, determining EGFR mutation status plays a crucial role in the selection of individuals who may potentially benefits from EGFR TKI treatment and predicting subsequent clinical outcomes [12]. However, the current clinical standard for EGFR genotyping, reliant on biopsy procedures, is invasive and prone to certain limitations. These limitations include patient reluctance, challenges related to the location or size, potential sampling errors, procedural complexities, extended testing durations, limited samples availability, compromised patient health, and spatial and temporal heterogeneity within the tumor [17, 18]. Alternative strategies such as radiogenetic analysis, may help overcome these limitations.

In this retrospective study, we investigated the feasibility of radiogenomics analysis to predict EGFR genotyping in 269 pretreated patients suffering solid lung adenocarcinoma. The sub-region-based machine learning classifier (classifier 2) outperformed the traditional whole-tumor-based machine learning classifier (classifier 1) with a higher AUC in the independent test group. Integration of the predictive probabilities from clinical features and sub-region Region of Interest (ROI) features, the combined radiogenomics model (classifier 4) demonstrated robust diagnostic performance. By incorporating radiomics metabolic features from ^{18}F-FDG PET, radiomics structural features from CT, relevant clinical factors, and sub-region-based radiomics, this study comprehensively explored the hybrid ^{18}F-FDG PET/CT image information to an unprecedented extent. Hence, the combined sub-region-based pretherapy hybrid ^{18}F-FDG PET/CT machine learning radiogenomics classifier could accurately predict EGFR mutation in solid lung adenocarcinoma, potentially serving as a noninvasive surrogate for traditional EGFR status test. It should be noted that the majority of EGFR mutations occur in hotspots between exons 18 and 20 [2]. However, targeted therapies are approved for patients with “classical” mutations and a small number of other mutations. Furthermore, effective therapies have not been identified for additional EGFR mutations [19]. Therefore, rare EGFR mutations were not included in this study.

In contradistinction to the general population of NSCLC patients, those harboring EGFR kinase domain mutations are more predisposed to being of Asian ethnicity, female gender, exhibiting adenocarcinoma histology, and having no history of smoking [4, 6]. Our study similarly identifies a lack of smoking history and female gender as predictors of EGFR mutation status. Notably, no statistically significant differences in terms of age and tumor stage were observed among distinct EGFR mutation groups (all $P > 0.05$).

^{18}F-FDG uptake on PET may be a noninvasive biomarker of underlying tumor genotypes. The EGFR gene mutation enhances glucose metabolism through the Akt signaling cascade in neoplastic cells, thereby inducing their proliferation and enhancing viability [20]. Subjective characteristics analysis depending on the naked eye or conventional ^{18}F-FDG PET parameters were most commonly used to predict EGFR mutation status in previous EGFR genotyping-related ^{18}F-FDG PET/CT researchers. Those studies have investigated the relationship between SUV_{max} measured from PET and led to contradictory results [6, 21]. Kim et al. found that all the metabolic and volumetric ^{18}F-FDG PET/CT values were significantly lower in EGFR mutant than EGFR wild type lung adenocarcinomas [22]. In current study, EGFR mutant subset showed lower SUV_{max} than EGFR wild subset. Various studies have identified specific SUV_{max} cutoff values indicative of EGFR mutation in NSCLC patients [6, 23-27]. Lv et al. [6] reported $SUV_{max} < 7.0$ as a predictor (AUC=0.557, n=849), Na et al. [28] $SUV_{max} < 9.2$ predictive (AUC=0.74, n=100), Mak et al. [29] observed $SUV_{max} < 5.0$ as a predictor (AUC=0.62, n=100), Cho et al. [30] identified $SUV_{max} < 9.6$ as predictive (AUC=0.68, n=61), and Guan et al. [31] determined $SUV_{max} < 8.1$ as predictive (AUC=0.65, n=316). Conversely, Ko et al. [31] established $SUV_{max} \geq 6$ (AUC=0.63, n=132) as predictive in lung adenocarcinoma, while Huang et al. [32] found $SUV_{max} \geq 9.5$ predictive (n=77).

However, those previous studies showed comparable inconsistency and relatively low discriminative abilities, because traditional PET parameters including SUV_{max} and SUV_{peak} do not include any spatial or texture information, which greatly reflecting EGFR mutation biology and tumor heterogeneity [33]. In the capacity of a hybrid imaging methodology, our ^{18}F-FDG PET/CT radiogenomic analysis derived radiomics characteristics from both CT and ^{18}F-FDG PET, thereby extensively harnessing imaging details through machine learning techniques. Currently, some radiogenomics studies on NSCLC EGFR mutation status have involved ^{18}F-FDG PET. Yip et al. [21] developed a 21 features-based radiomics model could distinguish the differences of tumor metabolic phenotypes caused by EGFR mutation and might potentially serve as noninvasive imaging biomarkers for somatic mutations. Rios et al. [27] analyzed the radiomic characteristics of 763 patients with lung adenocarcinoma from 4 medical centers and found that 16 features correlate with EGFR mutations. Li et al. [34] built a ^{18}F-FDG PET/CT-based radiogenomics signature for EGFR mutation classification reaching an AUC of 0.805, an accuracy of 80.798%, a sensitivity of 0.826, and a specificity of 0.783.

Failure to consider sub-region variations may reduce the diagnostic power of useful imaging biomarkers. By leveraging the most metabolically active sub-regional information of ^{18}F-FDG PET/CT, we proved the sub-region-based machine learning classifier outperformed traditional whole-tumor-based machine learning classifier, which is consistent with previous sub-regional radiomics analyses [11, 35]. After assessing copy number alterations, Xie et al. [9] further found that the sub-region-based CT

radiomics model have the potential to reflect esophageal tumor gene mutation. Furthermore, Xia et al. [35] constructed an eight sub-regional radiomics feature set for hepatocellular carcinoma, derived from enhanced CT values, and local entropy. These features were found to be significantly correlated with prognostic gene modules, with two of them specifically associated with overall survival (OS). However, the previous sub-region-based radiomics approaches extracted features from CT images only. Önner et al. [36] found that tumoral heterogeneity (TH) measurement with histogram-based textural features (HBTFs) may contribute to conventional metabolic parameters in guiding precision medicine for invasive lung adenocarcinoma (ILA). In present study, a brighter sub-region on ^{18}F-FDG PET indicating higher ^{18}F-FDG uptake was automatically segmented into sub-region ROIs using Otsu thresholding method, which applied to both ^{18}F-FDG PET and CT images for texture features extraction, involving not only underlying structural but also metabolic characteristics. Moreover, many previous researches proved the clinical factors potentially associated with EGFR mutation status [37]. Zhang et al. [38] found that combining radiomics features with clinical risk factors can yield added predictive value for EGFR mutation classification in NSCLC. In the present study, we integrated the prediction probability of clinical features and sub-region ROI features; the fused model showed a significantly better ability distinguishing EGFR mutants from the wild type, supporting the complementarity between clinical and radiomics features. Chang et al. [39] analyzed 583 cases of lung adenocarcinoma patients using ^{18}F-FDG PET/CT images. They found that the PET/CT radiomics-clinical combined model (AUC=0.84) outperformed the PET/CT radiomics model (AUC=0.76) and the clinical model (AUC=0.81) in predicting EGFR mutations. Wang et al. [40] analyzed CT images and EGFR gene sequencing data from 18,232 lung cancer patients across nine cohorts in China and the United States. In six retrospective and prospective testing cohorts, leveraging information extracted from CT images for the entire lung, a fully automated artificial intelligence system (FAIS) exhibited an AUC range of 0.748-0.813, surpassing commonly used tumor-based deep learning models. The FAIS, when combined with clinical factors (FAIS-C model), demonstrated a significant correlation between predicted genotypes and the prognosis of EGFR-TKI treatment. In this study, the combined classifier, which integrates sub-region analysis and clinical parameters, demonstrated improved predictive efficacy in determining EGFR mutation status compared to other classifiers. In comparison to previously reported research methodologies, although our results did not demonstrate a predictive efficacy surpassing other study protocols, it remains worthwhile to further validate this research approach, potentially utilizing larger sample sizes or even adopting a multicenter design.

There were several limitations to this study. First, this is a single-center study with limited sample size, which may introduce bias, compromise model's generalization ability, as well as affect its accuracy. Hence, it is necessary to formulate a prospective multi-center study with a larger population to validate this model. Second, the EGFR mutation status of only one tissue type (lung adenocarcinoma) was analyzed. Therefore, the predictive efficacy of this model in other lung cancer types necessitates further investigation.

Conclusion

This study substantiated that the integrated sub-region-based pretherapy ^{18}F-FDG PET/CT machine learning radiogenomics exhibited commendable predictive efficacy in discerning EGFR mutation status during the pretreatment phase of solid lung adenocarcinoma. This could potentially serve as a reasonably accurate, convenient, and noninvasive alternative to invasive biopsy for identifying suitable candidates for EGFR TKI therapy.

Acknowledgements

This study is supported by Medical Health Science and Technology Project of the Zhejiang Provincial Health Commission (2021KY563/2023KY068/2022PY043), and Zhejiang Province Natural Science Foundation of China (Grant number: LTGY24H180013).

Disclosure of conflict of interest

None.

Address correspondence to: Dr. Heqing Yi, Department of Nuclear Medicine, Zhejiang Cancer Hospital, Hangzhou 310022, Zhejiang, China. Tel: +86-571-88122332; Fax: +86-571-88122332; E-mail: yihq@zjcc.org.cn; yiheqing1989@163.com; Dr. Hongzhou Zhu, Department of Radiology, Zhejiang Cancer Hospital, Hangzhou 310022, Zhejiang, China. Tel: +86-571-88122222; Fax: +86-571-88122222; E-mail: zhuhz@zjcc.org.cn

References

[1] Sung H, Ferlay J, Siegel RL, Laversanne M, Soerjomataram I, Jemal A and Bray F. Global cancer statistics 2020: GLOBOCAN estimates of incidence and mortality worldwide for 36 cancers in 185 countries. CA Cancer J Clin 2021; 71: 209-249.

[2] Hsu WH, Yang JC, Mok TS and Loong HH. Overview of current systemic management of EGFR-mutant NSCLC. Ann Oncol 2018; 29: i3-i9.

[3] Kazandjian D, Blumenthal GM, Yuan W, He K, Keegan P and Pazdur R. FDA approval of gefitinib for the treatment of patients with metastatic EGFR mutation-positive non-small cell lung cancer. Clin Cancer Res 2016; 22: 1307-1312.

[4] Shi Y, Au JS, Thongprasert S, Srinivasan S, Tsai CM, Khoa MT, Heeroma K, Itoh Y, Cornelio G and Yang PC. A prospective, molecular epidemiology study of EGFR mutations in Asian patients with advanced non-small-cell lung cancer

of adenocarcinoma histology (PIONEER). J Thorac Oncol 2014; 9: 154-162.
[5] Wang S, Shi J, Ye Z, Dong D, Yu D, Zhou M, Liu Y, Gevaert O, Wang K, Zhu Y, Zhou H, Liu Z and Tian J. Predicting EGFR mutation status in lung adenocarcinoma on computed tomography image using deep learning. Eur Respir J 2019; 53: 1800986.
[6] Lv Z, Fan J, Xu J, Wu F, Huang Q, Guo M, Liao T, Liu S, Lan X, Liao S, Geng W and Jin Y. Value of (18)F-FDG PET/CT for predicting EGFR mutations and positive ALK expression in patients with non-small cell lung cancer: a retrospective analysis of 849 Chinese patients. Eur J Nucl Med Mol Imaging 2018; 45: 735-750.
[7] Caicedo C, Garcia-Velloso MJ, Lozano MD, Labiano T, Vigil Diaz C, Lopez-Picazo JM, Gurpide A, Zulueta JJ, Richter Echevarria JA and Perez Gracia JL. Role of [(1)(8)F]FDG PET in prediction of KRAS and EGFR mutation status in patients with advanced non-small-cell lung cancer. Eur J Nucl Med Mol Imaging 2014; 41: 2058-2065.
[8] Peng S, Spetsieris PG, Eidelberg D and Ma Y. Radiomics and supervised machine learning in the diagnosis of parkinsonism with FDG PET: promises and challenges. Ann Transl Med 2020; 8: 808.
[9] Xie C, Yang P, Zhang X, Xu L, Wang X, Li X, Zhang L, Xie R, Yang L, Jing Z, Zhang H, Ding L, Kuang Y, Niu T and Wu S. Sub-region based radiomics analysis for survival prediction in oesophageal tumours treated by definitive concurrent chemoradiotherapy. EBioMedicine 2019; 44: 289-297.
[10] Lv W, Zhou Z, Peng J, Peng L, Lin G, Wu H, Xu H and Lu L. Functional-structural sub-region graph convolutional network (FSGCN): application to the prognosis of head and neck cancer with PET/CT imaging. Comput Methods Programs Biomed 2023; 230: 107341.
[11] Wu J, Gensheimer MF, Dong X, Rubin DL, Napel S, Diehn M, Loo BW Jr and Li R. Robust intratumor partitioning to identify high-risk subregions in lung cancer: a pilot study. Int J Radiat Oncol Biol Phys 2016; 95: 1504-1512.
[12] Ettinger DS, Wood DE, Aisner DL, Akerley W, Bauman JR, Bharat A, Bruno DS, Chang JY, Chirieac LR, DeCamp M, Dilling TJ, Dowell J, Durm GA, Gettinger S, Grotz TE, Gubens MA, Hegde A, Lackner RP, Lanuti M, Lin J, Loo BW, Lovly CM, Maldonado F, Massarelli E, Morgensztern D, Ng T, Otterson GA, Patel SP, Patil T, Polanco PM, Riely GJ, Riess J, Schild SE, Shapiro TA, Singh AP, Stevenson J, Tam A, Tanvetyanon T, Yanagawa J, Yang SC, Yau E, Gregory KM and Hughes M. NCCN Guidelines® Insights: non-small cell lung cancer, version 2.2023. J Natl Compr Canc Netw 2023; 21: 340-350.
[13] Zwanenburg A, Vallières M, Abdalah MA, Aerts HJWL, Andrearczyk V, Apte A, Ashrafinia S, Bakas S, Beukinga RJ, Boellaard R, Bogowicz M, Boldrini L, Buvat I, Cook GJR, Davatzikos C, Depeursinge A, Desseroit MC, Dinapoli N, Dinh CV, Echegaray S, El Naqa I, Fedorov AY, Gatta R, Gillies RJ, Goh V, Götz M, Guckenberger M, Ha SM, Hatt M, Isensee F, Lambin P, Leger S, Leijenaar RTH, Lenkowicz J, Lippert F, Losnegard A, Maier-Hein KH, Morin O, Muller H, Napel S, Nioche C, Orlhac F, Pati S, Pfaehler EAG, Rahmim A, Rao AUK, Scherer J, Siddique MM, Sijtsema NM, Socarras Fernandez J, Spezi E, Steenbakkers RJHM, Tanadini-Lang S, Thorwarth D, Troost EGC, Upadhaya T, Valentini V, van Dijk LV, van Griethuysen J, van Velden FHP, Whybra P, Richter C and Lock S. The image biomarker standardization initiative: standardized quantitative radiomics for high-throughput image-based phenotyping. Radiology 2020; 295: 328-338.
[14] Boellaard R, Delgado-Bolton R, Oyen WJ, Giammarile F, Tatsch K, Eschner W, Verzijlbergen FJ, Barrington SF, Pike LC, Weber WA, Stroobants S, Delbeke D, Donohoe KJ, Holbrook S, Graham MM, Testanera G, Hoekstra OS, Zijlstra J, Visser E, Hoekstra CJ, Pruim J, Willemsen A, Arends B, Kotzerke J, Bockisch A, Beyer T, Chiti A and Krause BJ; European Association of Nuclear Medicine (EANM). FDG PET/CT: EANM procedure guidelines for tumour imaging: version 2.0. Eur J Nucl Med Mol Imaging 2015; 42: 328-354.
[15] Wu S, Zheng J, Li Y, Yu H, Shi S, Xie W, Liu H, Su Y, Huang J and Lin T. A radiomics nomogram for the preoperative prediction of lymph node metastasis in bladder cancer. Clin Cancer Res 2017; 23: 6904-6911.
[16] Li Q, Song Z, Li X, Zhang D, Yu J, Li Z, Huang J, Su K, Liu Q, Zhang X and Tang Z. Development of a CT radiomics nomogram for preoperative prediction of Ki-67 index in pancreatic ductal adenocarcinoma: a two-center retrospective study. Eur Radiol 2023; [Epub ahead of print].
[17] Fujii H, Nagakura H, Kobayashi N, Kubo S, Tanaka K, Watanabe K, Horita N, Hara Y, Nishikawa M, Miura K, Koizumi H, Ito Y, Tsubakihara M, Miyazawa N, Kudo M, Shinkai M and Kaneko T. Liquid biopsy for detecting epidermal growth factor receptor mutation among patients with non-small cell lung cancer treated with afatinib: a multicenter prospective study. BMC Cancer 2022; 22: 1035.
[18] Kim TO, Oh IJ, Kho BG, Park HY, Chang JS, Park CK, Shin HJ, Lim JH, Kwon YS, Kim YI, Lim SC, Kim YC and Choi YD. Feasibility of re-biopsy and EGFR mutation analysis in patients with non-small cell lung cancer. Thorac Cancer 2018; 9: 856-864.
[19] Robichaux JP, Le X, Vijayan RSK, Hicks JK, Heeke S, Elamin YY, Lin HY, Udagawa H, Skoulidis F, Tran H, Varghese S, He J, Zhang F, Nilsson MB, Hu L, Poteete A, Rinsurongkawong W, Zhang X, Ren C, Liu X, Hong L, Zhang J, Diao L, Madison R, Schrock AB, Saam J, Raymond V, Fang B, Wang J, Ha MJ, Cross JB, Gray JE and Heymach JV. Structure-based classification predicts drug response in EGFR-mutant NSCLC. Nature 2021; 597: 732-737.
[20] Li Z, Jiang Y, Liu J, Fu H, Yang Q, Song W and Li Y. Exosomes from PYCR1 knockdown bone marrow mesenchymal stem inhibits aerobic glycolysis and the growth of bladder cancer cells via regulation of the EGFR/PI3K/AKT pathway. Int J Oncol 2023; 63: 84.
[21] Yip SS, Kim J, Coroller TP, Parmar C, Velazquez ER, Huynh E, Mak RH and Aerts HJ. Associations between somatic mutations and metabolic imaging phenotypes in non-small cell lung cancer. J Nucl Med 2017; 58: 569-576.
[22] Kim YI, Paeng JC, Park YS, Cheon GJ, Lee DS, Chung JK and Kang KW. Relation of EGFR mutation status to metabolic activity in localized lung adenocarcinoma and its influence on the use of FDG PET/CT parameters in prognosis. AJR Am J Roentgenol 2018; 210: 1346-1351.
[23] Suzuki H, Sasaki E, Tamaki T, Kodaira T, Nishio M, Nishikawa D, Beppu S, Terada H, Sawabe M and Hanai N. Association between ^{18}F-Fluorodeoxyglucose uptake and mutation status of epidermal growth factor receptor in sinonasal tract cancer. Anticancer Res 2023; 43: 3247-3253.

[24] Gao J, Shi Y, Niu R, Shao X and Shao X. Association analysis of maximum standardized uptake values based on (18) F-FDG PET/CT and EGFR mutation status in lung adenocarcinoma. J Pers Med 2023; 13: 396.
[25] Ko KH, Hsu HH, Huang TW, Gao HW, Shen DH, Chang WC, Hsu YC, Chang TH, Chu CM, Ho CL and Chang H. Value of (1)(8)F-FDG uptake on PET/CT and CEA level to predict epidermal growth factor receptor mutations in pulmonary adenocarcinoma. Eur J Nucl Med Mol Imaging 2014; 41: 1889-1897.
[26] Gao J, Niu R, Shi Y, Shao X, Jiang Z, Ge X, Wang Y and Shao X. The predictive value of [(18)F]FDG PET/CT radiomics combined with clinical features for EGFR mutation status in different clinical staging of lung adenocarcinoma. EJNMMI Res 2023; 13: 26.
[27] Rios Velazquez E, Parmar C, Liu Y, Coroller TP, Cruz G, Stringfield O, Ye Z, Makrigiorgos M, Fennessy F, Mak RH, Gillies R, Quackenbush J and Aerts HJWL. Somatic mutations drive distinct imaging phenotypes in lung cancer. Cancer Res 2017; 77: 3922-3930.
[28] Na II, Byun BH, Kim KM, Cheon GJ, Choe du H, Koh JS, Lee DY, Ryoo BY, Baek H, Lim SM, Yang SH, Kim CH and Lee JC. ^{18}F-FDG uptake and EGFR mutations in patients with non-small cell lung cancer: a single-institution retrospective analysis. Lung Cancer 2010; 67: 76-80.
[29] Mak RH, Digumarthy SR, Muzikansky A, Engelman JA, Shepard JA, Choi NC and Sequist LV. Role of ^{18}F-fluorodeoxyglucose positron emission tomography in predicting epidermal growth factor receptor mutations in non-small cell lung cancer. Oncologist 2011; 16: 319-326.
[30] Cho A, Hur J, Moon YW, Hong SR, Suh YJ, Kim YJ, Im DJ, Hong YJ, Lee HJ, Kim YJ, Shim HS, Lee JS, Kim JH and Choi BW. Correlation between EGFR gene mutation, cytologic tumor markers, ^{18}F-FDG uptake in non-small cell lung cancer. BMC Cancer 2016; 16: 224.
[31] Guan J, Xiao NJ, Chen M, Zhou WL, Zhang YW, Wang S, Dai YM, Li L, Zhang Y, Li QY, Li XZ, Yang M, Wu HB, Chen LH and Liu LY. ^{18}F-FDG uptake for prediction EGFR mutation status in non-small cell lung cancer. Medicine (Baltimore) 2016; 95: e4421.
[32] Huang CT, Yen RF, Cheng MF, Hsu YC, Wei PF, Tsai YJ, Tsai MF, Shih JY, Yang CH and Yang PC. Correlation of F-18 fluorodeoxyglucose-positron emission tomography maximal standardized uptake value and EGFR mutations in advanced lung adenocarcinoma. Med Oncol 2010; 27: 9-15.
[33] Cook GJR, Azad G, Owczarczyk K, Siddique M and Goh V. Challenges and promises of PET radiomics. Int J Radiat Oncol Biol Phys 2018; 102: 1083-1089.
[34] Li X, Yin G, Zhang Y, Dai D, Liu J, Chen P, Zhu L, Ma W and Xu W. Predictive power of a radiomic signature based on (18)F-FDG PET/CT images for EGFR mutational status in NSCLC. Front Oncol 2019; 9: 1062.
[35] Xia W, Chen Y, Zhang R, Yan Z, Zhou X, Zhang B and Gao X. Radiogenomics of hepatocellular carcinoma: multiregion analysis-based identification of prognostic imaging biomarkers by integrating gene data-a preliminary study. Phys Med Biol 2018; 63: 035044.
[36] Önner H, Coşkun N, Erol M and Eren Karanis MI. The role of histogram-based textural analysis of (18)F-FDG PET/CT in evaluating tumor heterogeneity and predicting the prognosis of invasive lung adenocarcinoma. Mol Imaging Radionucl Ther 2022; 31: 33-41.
[37] Qin X, Wang H, Hu X, Gu X and Zhou W. Predictive models for patients with lung carcinomas to identify EGFR mutation status via an artificial neural network based on multiple clinical information. J Cancer Res Clin Oncol 2020; 146: 767-775.
[38] Zhang L, Chen B, Liu X, Song J, Fang M, Hu C, Dong D, Li W and Tian J. Quantitative biomarkers for prediction of epidermal growth factor receptor mutation in non-small cell lung cancer. Transl Oncol 2018; 11: 94-101.
[39] Chang C, Zhou S, Yu H, Zhao W, Ge Y, Duan S, Wang R, Qian X, Lei B, Wang L, Liu L, Ruan M, Yan H, Sun X and Xie W. A clinically practical radiomics-clinical combined model based on PET/CT data and nomogram predicts EGFR mutation in lung adenocarcinoma. Eur Radiol 2021; 31: 6259-6268.
[40] Wang S, Yu H, Gan Y, Wu Z, Li E, Li X, Cao J, Zhu Y, Wang L, Deng H, Xie M, Wang Y, Ma X, Liu D, Chen B, Tian P, Qiu Z, Xian J, Ren J, Wang K, Wei W, Xie F, Li Z, Wang Q, Xue X, Liu Z, Shi J, Li W and Tian J. Mining whole-lung information by artificial intelligence for predicting EGFR genotype and targeted therapy response in lung cancer: a multicohort study. Lancet Digit Health 2022; 4: e309-e319.